

## Electronic Supplementary Information

### Imidazolate-Mediated Assembled Structures of Co-LDH Sheets for Efficient Electrocatalytic Oxygen Evolution

Liyong Chen,<sup>\*,†</sup> Yuting Guo,<sup>†</sup> Huifang Wang,<sup>†</sup> Zhizhi Gu,<sup>†</sup> Yingyue Zhang,<sup>†</sup> Xuezhao Li,<sup>†</sup> Hong Wang,<sup>\*,‡</sup> and Chunying Duan<sup>\*,†</sup>

<sup>†</sup>State Key Laboratory of Fine Chemicals, Dalian University of Technology, 2 Linggong RD., Dalian, 116024,

<sup>‡</sup>China Institute of Advanced Synthesis (IAS), School of Chemistry and Molecular Engineering, Nanjing Tech University, Nanjing, 211816, China

E-mail: lychen@dlut.edu.cn; cyduan@dlut.edu.cn; ias\_hwang@njtech.edu.cn

### Experimental Section

#### Materials and characterization methods

All chemical reagents were used as received. Nafion solution (5 wt% in mixture of water and 2-propanol) was purchased from Sigma Aldrich, and other chemicals and solvents, including cobalt nitrate ( $\text{Co}(\text{NO}_3)_2 \cdot 6\text{H}_2\text{O}$ ), imidazole, 2-methylimidazole (Hmim), 2-ethylimidazole, benzimidazole, sodium hydroxide (NaOH), potassium hydroxide (KOH), methanol, ethanol, *n*-propanol and ethylene glycol, were purchased from Sinopharm Chemical Reagent Co., Ltd, China.

Transmission electron microscopy (TEM) was performed for microstructural and morphological investigation with a Tecnai F30 operated at 300 kV. Scanning electron microscopy (SEM) was performed for structural and morphological investigation on

HITACHI UHR FE-SEM SU8220. X-ray diffraction (XRD) was carried out in a Rigaku D/Max 2400 automatic powder X-ray diffractometer with Cu- $K\alpha$  radiation ( $\lambda = 1.5418 \text{ \AA}$ ). Atomic force microscopy (AFM) was used to measure the thickness of sheets on Park Systems XE-70 with non-contact mode. The content of cobalt was evaluated by inductively coupled plasma atomic emission spectroscopy (ICP-AES) on Optima 2000DV. X-ray photoelectron spectroscopy (XPS) was used to analyze surface elemental composition and chemical state of samples on Thermo ESCALAB 250Xi with Al-  $K\alpha$  radiation ( $h\nu = 1486.6 \text{ eV}$ ). Linear-sweep voltammetry (LSV), cyclic voltammetry (CV), and chronoamperometry were measured on a CHI760E electrochemical workstation with a typical three-electrode cell. Electrochemical impedance spectroscopy (EIS) was collected on a ZAHNER ENNIUM electrochemical workstation with a typical three-electrode cell.

## **Materials synthesis**

*Preparation of ZIF-67 rhombic dodecahedra (RDs).* In a typical synthetic procedure,  $\text{Co}(\text{NO}_3)_2$  (0.6 mmol) and Hmim (1.2 mmol) were dispersed into methanol (7.5 mL), respectively; subsequently,  $\text{Co}(\text{NO}_3)_2$  solution was slowly poured into Hmim solution with vigorously stirring. The resulting mixture in 20 mL of vial was kept at room temperature for 24 h without turbulence. The final dark violet product was rinsed twice by methanol, and dried in vacuum at  $100 \text{ }^\circ\text{C}$  for 12 h before further characterization.

In the preparation procedure, ethanol was used to replace methanol to test solvent effect on production of ZIF-67 while other conditions were kept unchanged.

*Preparation of porous Co-LDHs (referred to Co-LDH-1).*  $\text{Co}(\text{NO}_3)_2$  (0.6 mmol) and Hmim (1.2 mmol) were sequentially added into a 20 mL of Teflon-lined stainless steel autoclave containing 15 mL of methanol with stirring, and subsequently heated at 100 °C for 4 h. The yellowish brown powder was rinsed twice by methanol, and dried in vacuum at 100 °C for 12 h before further characterization.

The synthetic experiments were performed while substituting methanol with ethanol, *n*-propanol, ethylene glycol, and water, respectively. It is noted that the reaction temperature was increased to 120 °C if ethylene glycol was used as solvent. In the synthetic experiments, imidazole, 2-ethylimidazole, and benzimidazole were also used to substitute for Hmim under otherwise identical conditions when methanol was served as the reaction medium.

*Preparation of ZIF-67 RDs by transformation of Co-LDHs-1.* The as-synthesized porous Co-LDHs (mole of cobalt = 0.6 mmol, calculation according to ICP-AES) were dispersed in methanol (15 mL) containing Hmim (1.2 mmol), and kept at room temperature for 10 d with gently stirring. The dark violet powder obtained was rinsed twice by methanol, and dried in vacuum at 100 °C for 12 h before further characterization.

Non-purified Co-LDHs-1 was directly applied to the transformation experiment to prepared ZIF-67 RDs by the same procedure. In detail, Hmim (1.2 mmol) was introduced to the synthetic system of Co-LDHs-1 (15 mL); subsequently, the mixture was kept at room temperature for 10 d with gently stirring. Note the mole of  $\text{Co}^{2+}$  was evaluated based on the amount of  $\text{Co}(\text{NO}_3)_2$  added in the preparation process of Co-LDHs-1.

*Preparation of cage-like Co-LDH (referred to Co-LDH-2) by transformation of ZIF-67.*

The as-synthesized ZIF-67 RDs (0.6 mmol) were dispersed in methanol (15 mL), and then heated at 100 °C for 4 d by a solvothermal process. The final yellowish brown powder was rinsed twice by ethanol, and dried in vacuum at 100 °C for 12 h before further characterization.

Alternatively, non-purified ZIF-67 RDs were directly used to prepare Cage-like Co-LDHs via solvothermal treatment at 100 °C for 4 d.

*Preparation of ZIF-67 RDs by a cycling transformation route.* The non-purified ZIF-67 RDs in the synthetic system (15 mL) were directly heated at 100 °C for 4 d through a solvothermal process. Afterwards, the yellowish brown intermediate of Co-LDHs was incubated at room temperature for 10 d with gently stirring after introducing Hmim (1.2 mmol). Finally, the dark violet powder obtained was washed twice by methanol, and dried in vacuum at 100 °C for 12 h before further characterization.

*Preparation of cage-like Co-LDHs by a cycling transformation route.* The non-purified porous Co-LDHs in the synthetic system (15 mL) were directly incubated at room temperature for 10 d with gently stirring after introducing Hmim (1.2 mmol). Subsequently, the dark violet intermediate of ZIF-67 was heated at 100 °C for 4 d through a solvothermal process. Finally, the yellowish brown powder obtained was washed twice by methanol, and dried in vacuum at 100 °C for 12 h before further characterization.

*Preparation of dispersive Co-LDH (referred to d-Co-LDH) sheets.* The as-synthesized Co-LDHs (50 mg) were dispersed into formamide (50 mL), and the mixture was sonicated for 30 min using a probe sonicator (JY92-IIN Ultrasonic Homogenizer, 650 W, 30%) and then stirred for 8 h. The final samples were separated by centrifugation at 3000 rpm to discard the solid, and subsequently the supernatant was collected by centrifugation at 13300 rpm. The resulting *d*-Co-LDH sheets were subjected to characterization after being washed with methanol. Note that both *d*-Co-LDH samples were defined as *d*-Co-LDHs-1 and *d*-Co-LDHs-2, which were derived from Co-LDHs-1 and -2, respectively.

## **Electrochemical measurements**

*Preparation of electrocatalyst inks:* Electrocatalysts (5 mg) were dispersed into the mixture of water and 2-propanol with volume ratio of 1:1 (0.975 mL), and then Nafion solution (0.025

mL, 5 wt%) was added. The final mixture was sonicated in an ultrasonic bath for 20 min to form a well-dispersed suspension.

*Preparation of work electrodes:* Prior to utilization, glassy carbon (GC) electrodes (3 mm in diameter) were firstly polished with alumina suspension in deionized water on a Nylon plate; subsequently, the polished GC electrodes were rinsed with deionized water. Carbon fiber papers (CFPs) were sequentially treated by sonication in HNO<sub>3</sub>, H<sub>2</sub>O, ethanol and acetone for 30 min, respectively. Afterwards, a tape was used to define an area of 0.09 cm<sup>2</sup>. The resultant electrocatalyst ink (5 μL) was drop-casted on the surface of a glassy carbon electrode or a CFP electrode. All electrodes prepared were dried at room temperature in air for 1 h. The GC/CFP electrodes loading electrocatalysts were used as the working electrode. Hg/HgO (1 M KOH) and polished Pt wire were used as the reference electrode and the counter electrode in a three-electron cell, respectively.

*Electrochemical measurement:* LSV tests were performed in 1 M KOH solution at a sweep rate of 5 mV s<sup>-1</sup> with a potential window of 0 to 0.8 V vs Hg/HgO after 5 CV scans between 0 V and 0.6 V. CV tests were carried out in 1 M KOH solution at variable sweep rate from 20 to 120 mV s<sup>-1</sup> with an increment of 20 mV s<sup>-1</sup> with a potential window of 0.3 to 0.4 V vs Hg/HgO to measure the double-layer capacitance of electrocatalysts. Cycling stability of electrocatalysts was evaluated by successively scanning CV 3000 times with a potential window of 0.3 to 0.6 V vs Hg/HgO at a sweep rate of 10 mV s<sup>-1</sup>. EIS was collected in 1 M

KOH solution at overpotential of 395 mV in the frequency range from 0.1 Hz to 100 kHz with oscillation potential amplitudes of 5 mV. The aforementioned electrochemical tests were used GC electrodes as the work electrode in a three-electrode cell. Long-term stability for electrocatalysts on CFP electrodes was further investigated by chronoamperometry tests for 8 h after 5 CV scans between 0 V and 0.6 V vs Hg/HgO in 1 M KOH solution. During the measuring process, the overpotentials were fixed at 300 mV for *d*-Co-LDHs-1 and -2 and 330 mV for Co-LDHs-1 and -2.

The Tafel plots were calculated by LSV curves based on an equation of  $\eta = a + blg j$ . The potentials vs reversible hydrogen electrode (RHE) were obtained by converting the measured potentials vs Hg/HgO using the Nernst equation of  $E_{\text{RHE}} = E_{\text{Hg/HgO}} + 0.0591\text{pH} + 0.098$

**Table S1.** Comparison of the electrocatalytic activity of cobalt-based LDHs towards OER.

Catalyst	Preparation Method	Electrolyte	Onset Potential [V]	Current Density [mA cm <sup>-2</sup> ]	$\eta$ (at corresponding current density) [V]	Tafel Slope [mV dec <sup>-1</sup> ]	Ref
Co-LDH	Solvothermal	1M KOH	~1.47	10	0.312/0.319/0.321	68.4/77.7/77.9	This work
<i>m</i> -CO-LDH	Solvothermal	1M KOH	~1.45	10	0.288/0.289/0.29	55.1/57.0/60.9	This work
Exfoliated CoFe-LDH	Hydrothermal	1M KOH	1.457	10	0.266	37.85	1
Exfoliated CoCo(NiCo/NiFe)-LDH	Topochemical approach	1M KOH	—	10	0.35(0.33/0.3)	45(41/40)	2
NiCo-LDH/NF	Solvothermal	1M KOH	1.7	10	0.271	72	3
NiCo-LDH	Solvothermal	0.1M KOH	1.52	10	0.42	113	4
Exfoliated NiCo-LDH	Hydrothermal continuous-flow synthesis	1M KOH	—	10	0.367	40	5
NiCoFe-LDH	Hydrothermal	1M KOH	1.46	80	0.257	53	6
CoMn-LDH	Co-precipitation	1M KOH	—	10	0.324	43	7
NiCo-LDH/N-G	Hydrothermal	0.1M KOH	1.58	—	—	614	8
ZnCo-LDH	Microwave-assisted approach	0.1M KOH	1.46	2	0.375	101	9
ZnCo-LDH	Electrodeposition	0.1M KOH	1.56	2	0.427	83	10
ZnCo-LDH/G	Co-precipitation	0.1M KOH	1.56	10	0.43	73	11
CoFe-LDH-F	Hydrothermal	1M KOH	—	10	0.3	40	12
NiFe-LDH-rGO	Topochemical oxidation	1M KOH	—	10	0.21	40	13
3DGN/CoAl-LDH	Hydrothermal	1M KOH	—	10	0.252	36	14
Exfoliated CoFe-LDH	Hydrothermal	1M KOH	—	10	0.232	36	15

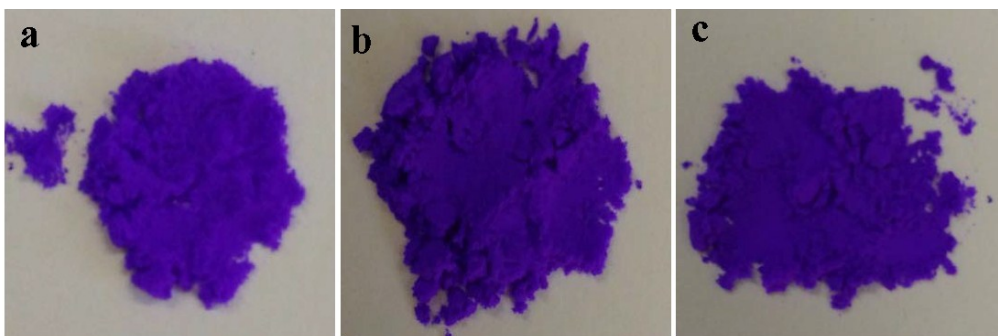


**Fig. S1.** The optical images of ZIF-67 prepared by (a) mixing  $\text{Co}(\text{NO}_3)_2$  and Hmim in methanol at room temperature, (b) transformation of Co-LDHs-1 and (c) cycling transformation from non-purified ZIF-67 to Co-LDHs to ZIF-67.

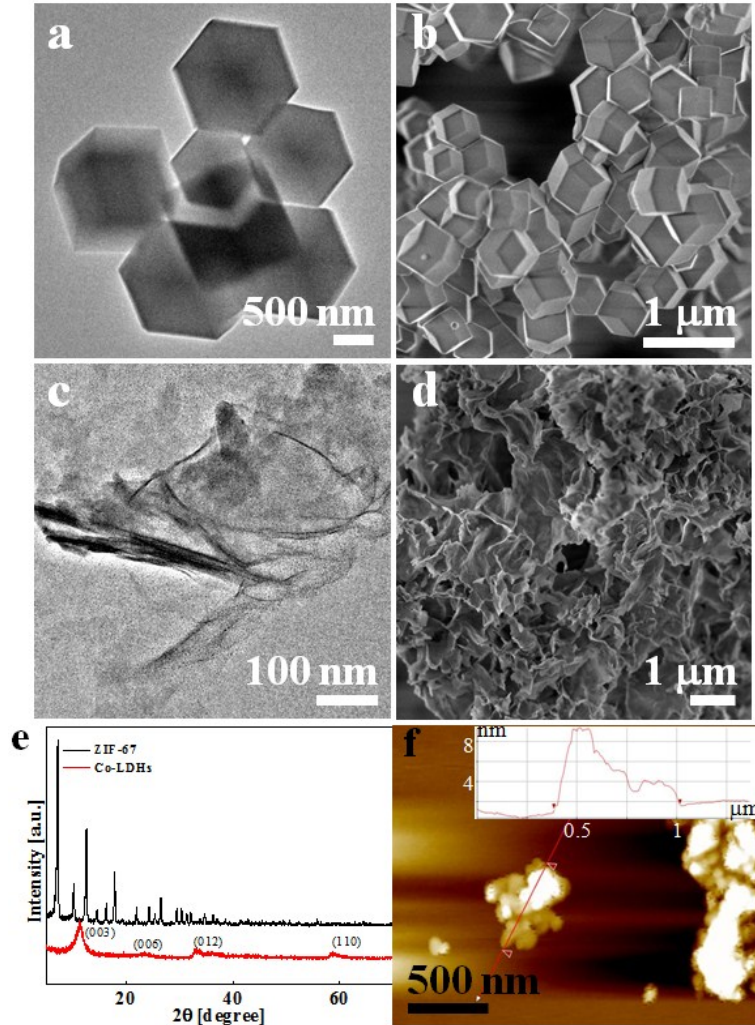


**Fig. S2.** TEM images and SEM images of (a, b) ZIF-67 RDs and (c, d) Co-LDHs-1 by mixing  $\text{Co}(\text{NO}_3)_2$  and Hmim in methanol at room temperature for 24 h and at 100 °C for 4 h, respectively; (e) the corresponding XRD patterns; (f) AFM image of Co-LDH sheets that were prepared by suctioning the supernatant after sonication of Co-LDH-1 in ethanol with an ultrasonic bath for 30 min and centrifugation at 3000 rpm.

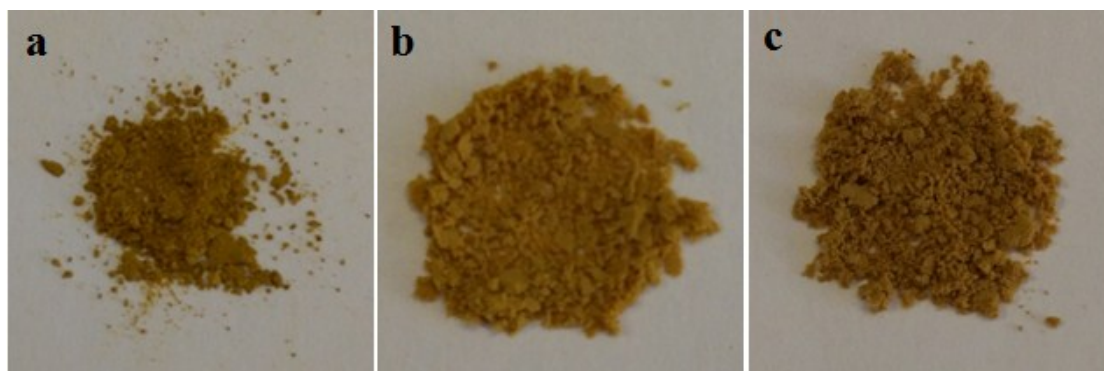


**Fig. S3.** The optical images of Co-LDHs prepared by (a) solvothermal treatment of  $\text{Co}(\text{NO}_3)_2$  and Hmim in methanol, (b) transformation of ZIF-67 and (c) cycling transformation from non-purified Co-LDHs to ZIF-67 to Co-LDHs.

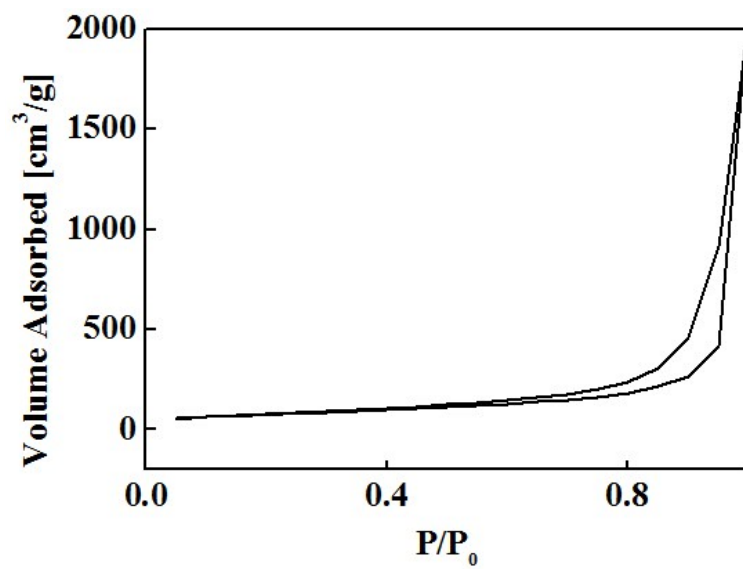


**Fig. S4.** N<sub>2</sub> physisorption isotherm of Co-LDHs-1 at 77 K.

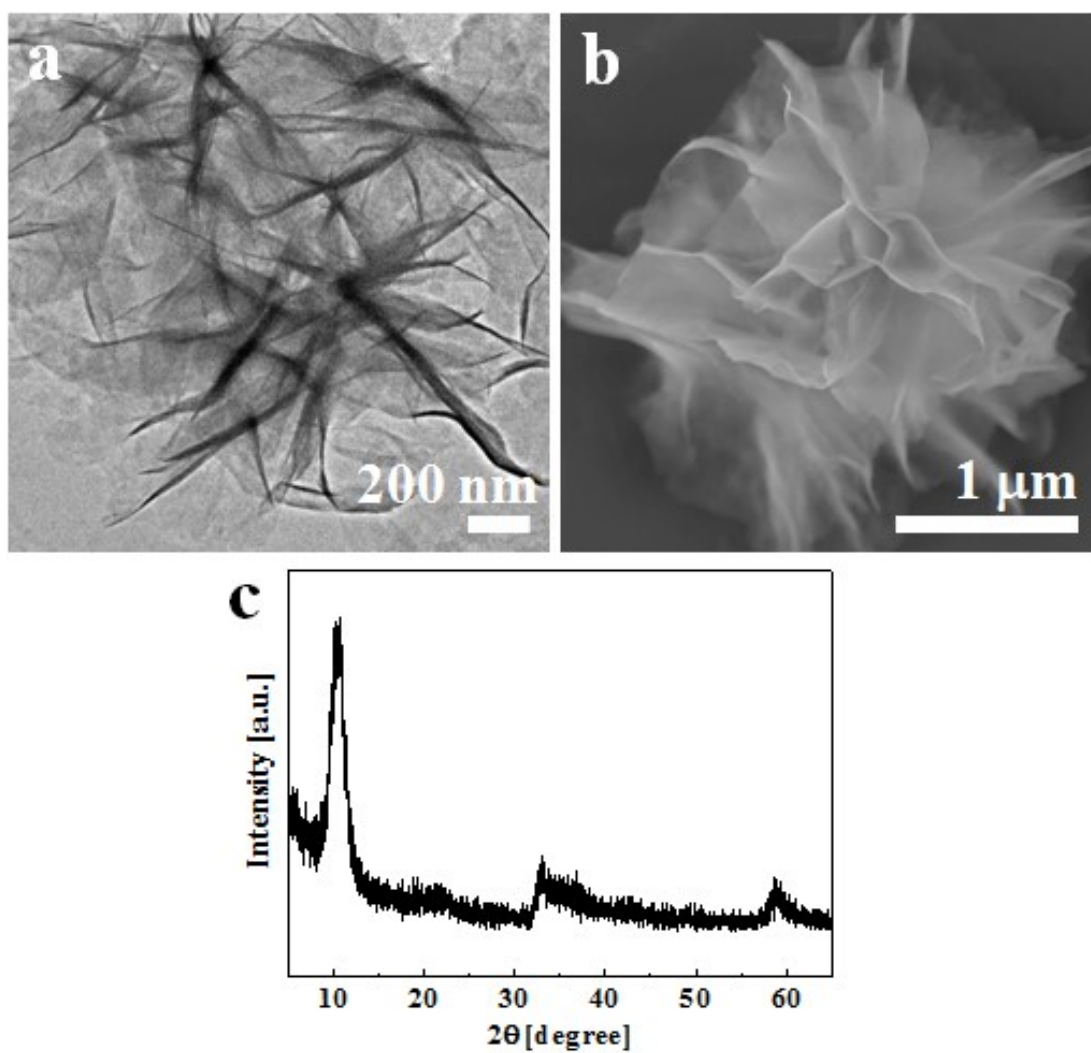


**Fig. S5.** (a) TEM image, (b) SEM image and (c) XRD pattern of Co-LDHs by solvothermal treatment of methanolic solution of  $\text{Co}(\text{NO}_3)_2$  and 2-ethylimidazole at 100 °C for 4 h.

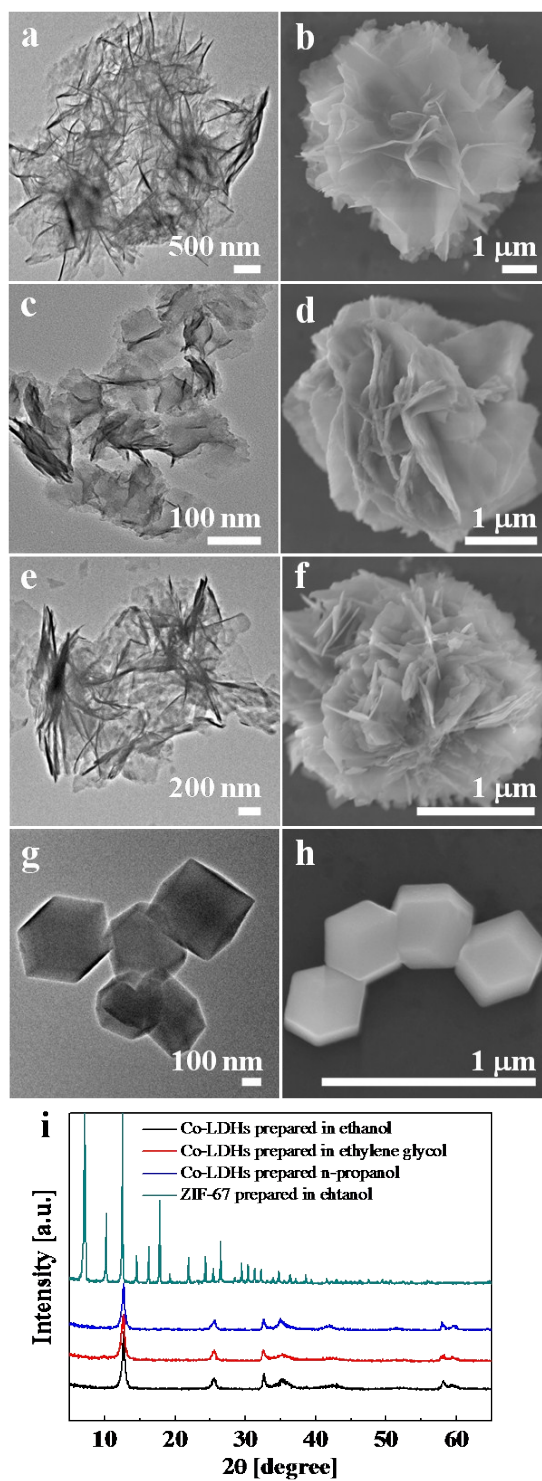


**Fig. S6.** TEM images (left) and SEM images (right) of Co-LDHs prepared in (a, b) ethanol, (c, d) ethylene glycol and (e, f) *n*-propanol and ZIF-67 prepared in (g, h) ethanol; (i) XRD patterns of corresponding samples (from bottom to top).

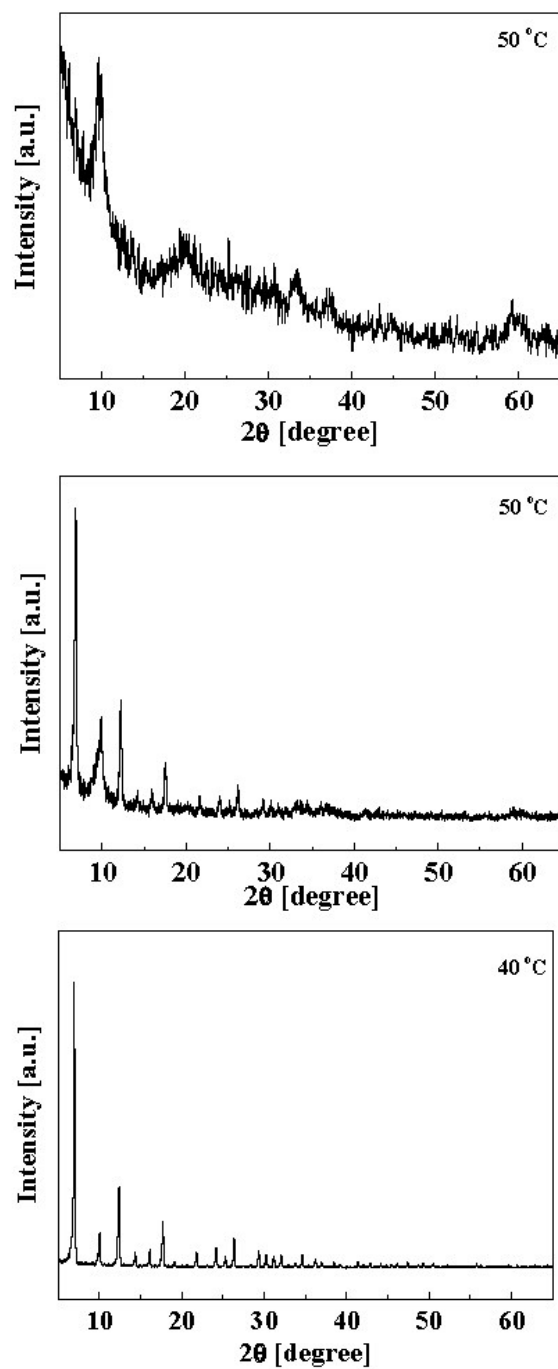


**Fig. S7.** XRD patterns of the samples prepared by thermal treatment of the methanolic solution of  $\text{Co}(\text{NO}_3)_2$  and Hmim under different conditions: at 50 °C for 24 h (top), at 50 °C for 4 h (middle), and at 40 °C for 24 h (bottom).

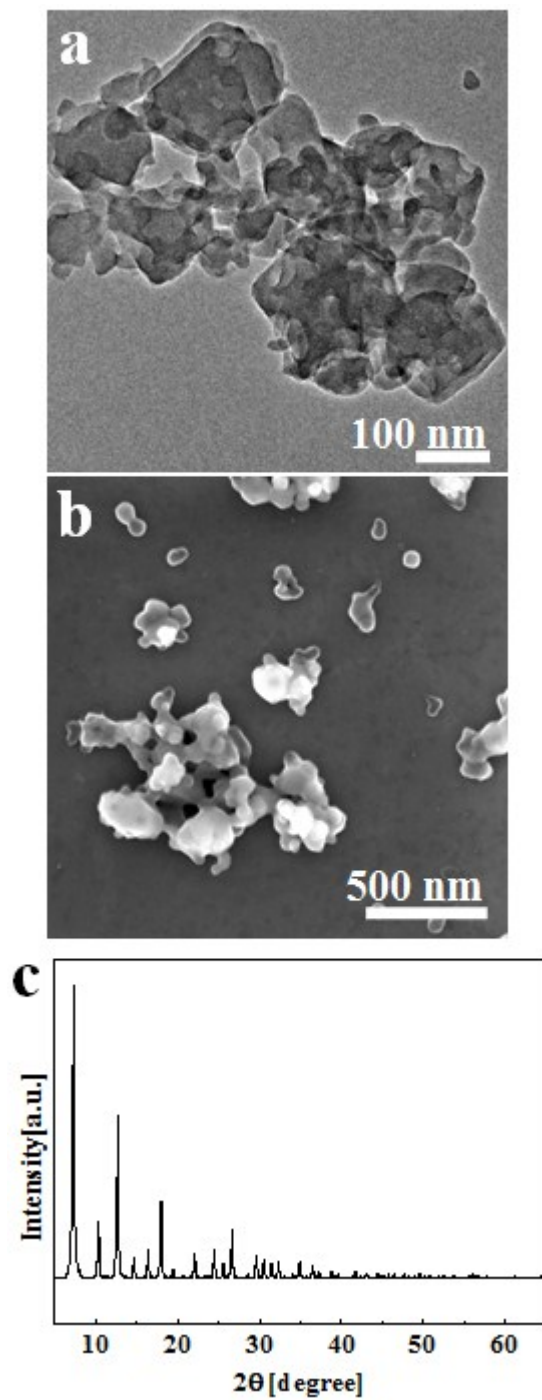


**Fig. S8.** (a) TEM image, (b) SEM image and (c) XRD pattern of the sample prepared from a methanolic solution of  $\text{Co}(\text{NO}_3)_2$ , Hmim and NaOH at room temperature for 24 h.

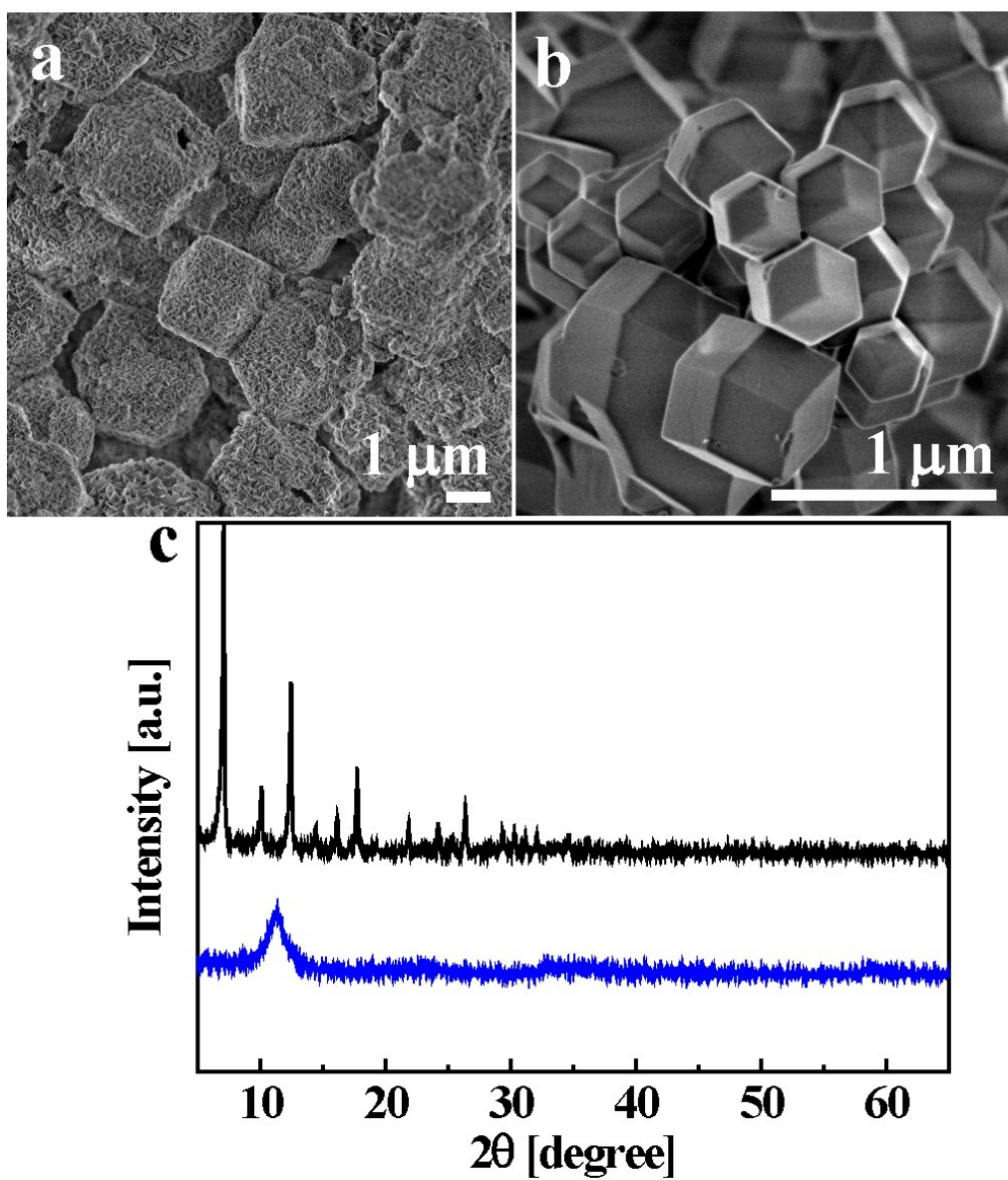


**Fig. S9.** SEM images of (a) Co-LDHs-2 and (b) ZIF-67 RDs based on the transformation route; (c) XRD patterns of Co-LDHs-2 (blue curve) and ZIF-67 RDs (black curve).

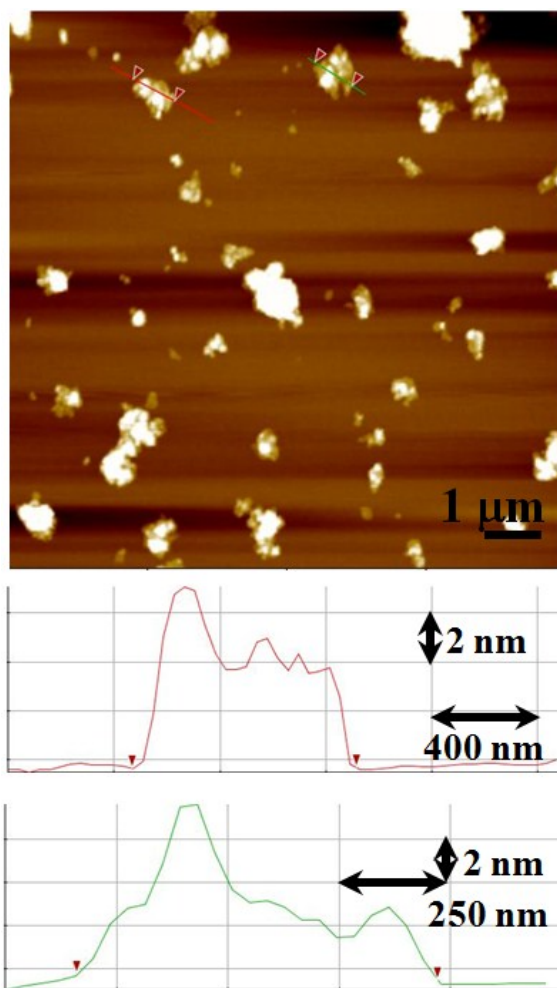


**Fig. S10.** AFM image of Co-LDH sheets that were prepared by suctioning the supernatant after sonication of the Co-LDHs-2 in ethanol with an ultrasonic bath for 30 min and centrifugation at 3000 rpm.

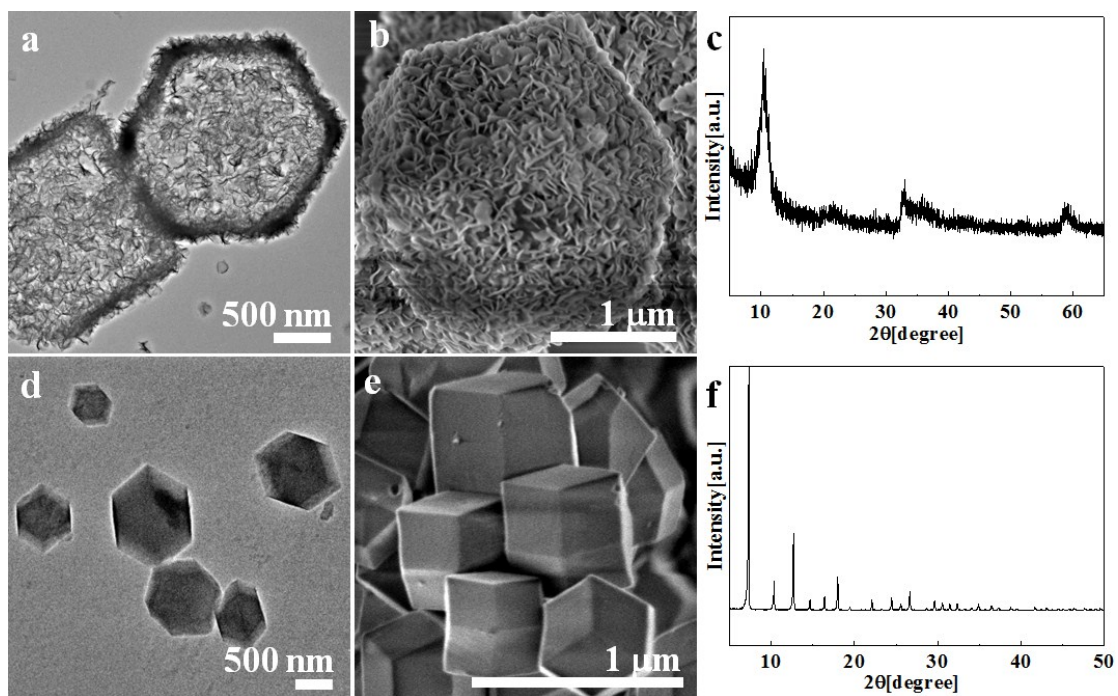


**Fig. S11.** TEM and SEM images of (a, b) cage-like Co-LDHs and (d, e) ZIF-67 RDs obtained by the transformation route involving their respective solid precursors without separation from synthetic systems; XRD patterns of (c) cage-like Co-LDHs and (f) ZIF-67 RDs.

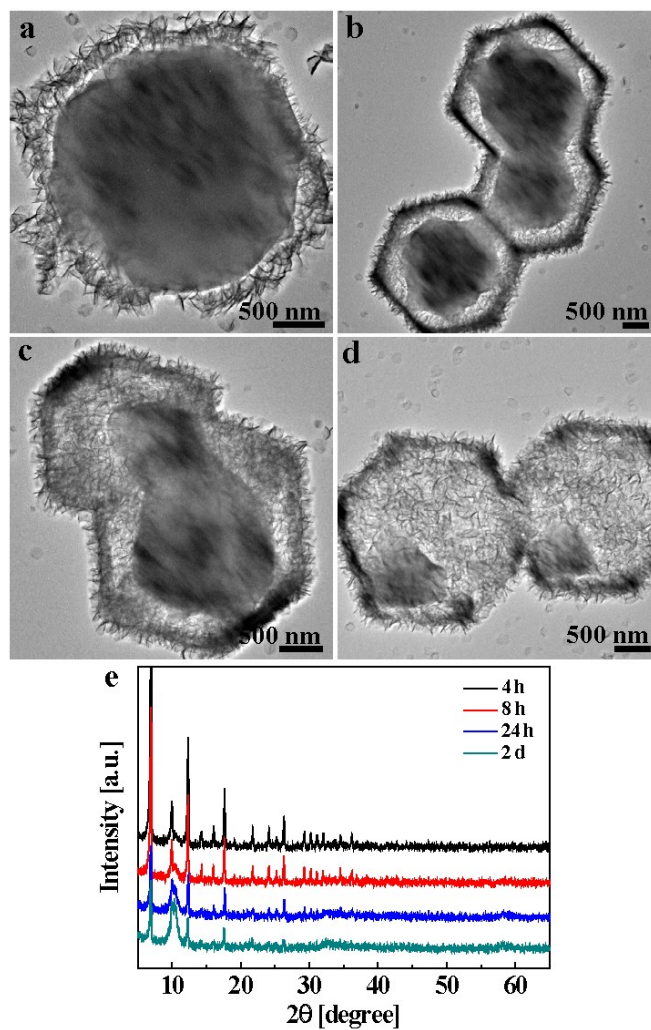


**Fig. S12.** Ex-situ TEM images of intermediates captured at (a) 4 h, (b) 8 h, (c) 24 h and (d) 2 d in the transformation process from purified ZIF-67 to Co-LDHs; (e) XRD patterns of these intermediates.

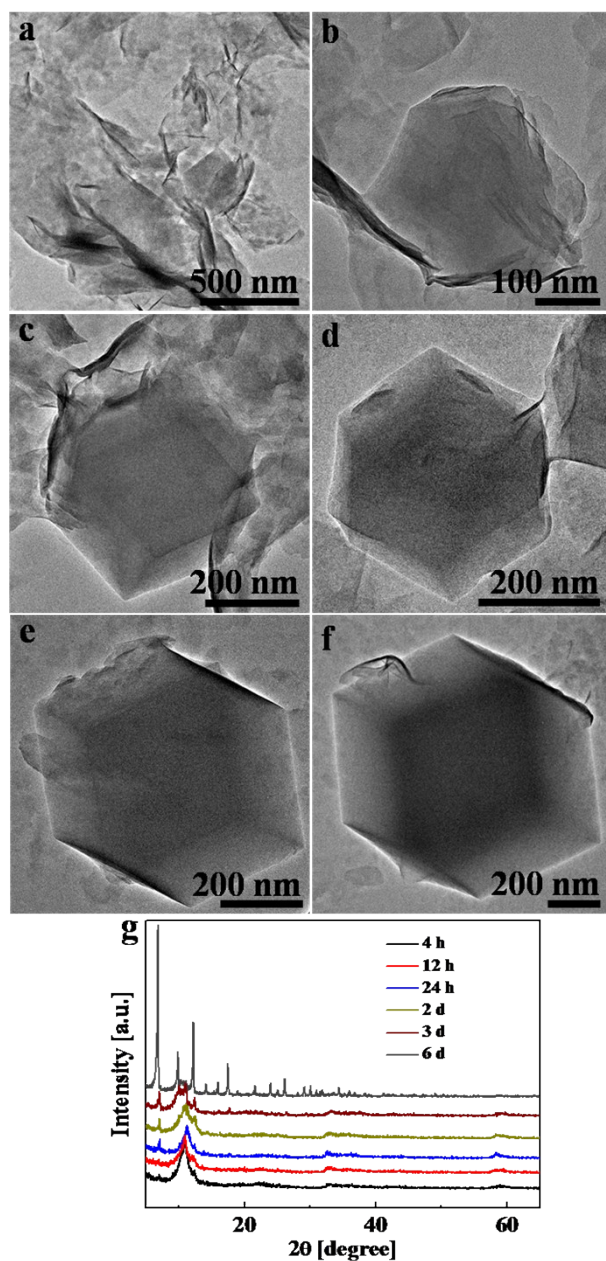


**Fig. S13.** Ex-situ TEM images of intermediates captured at (a) 4 h, (b) 12 h, (c) 24 h, (d) 2d, (e) 3 d and (f) 6 d in the transformation process from purified Co-LDHs to ZIF-67; (g) XRD patterns of the intermediates.

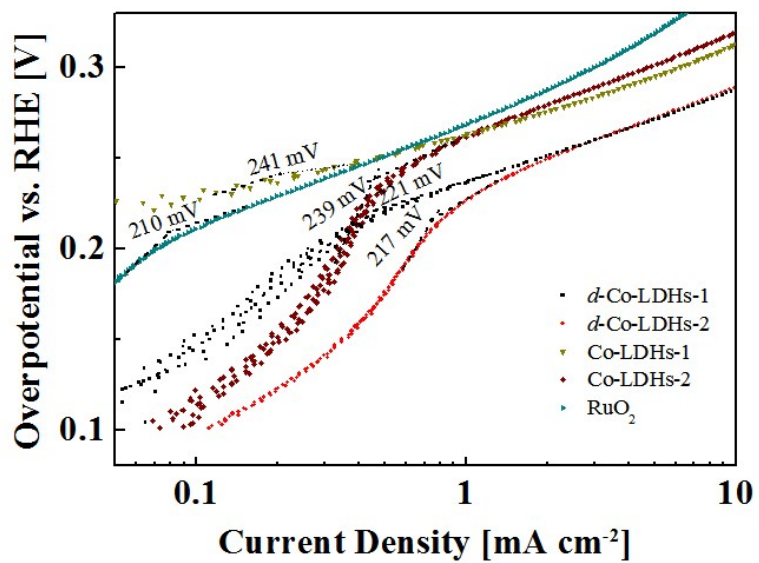


**Fig. S14.** Derivative LSV curves at low current density to evaluate the onset potential of electrocatalysts.

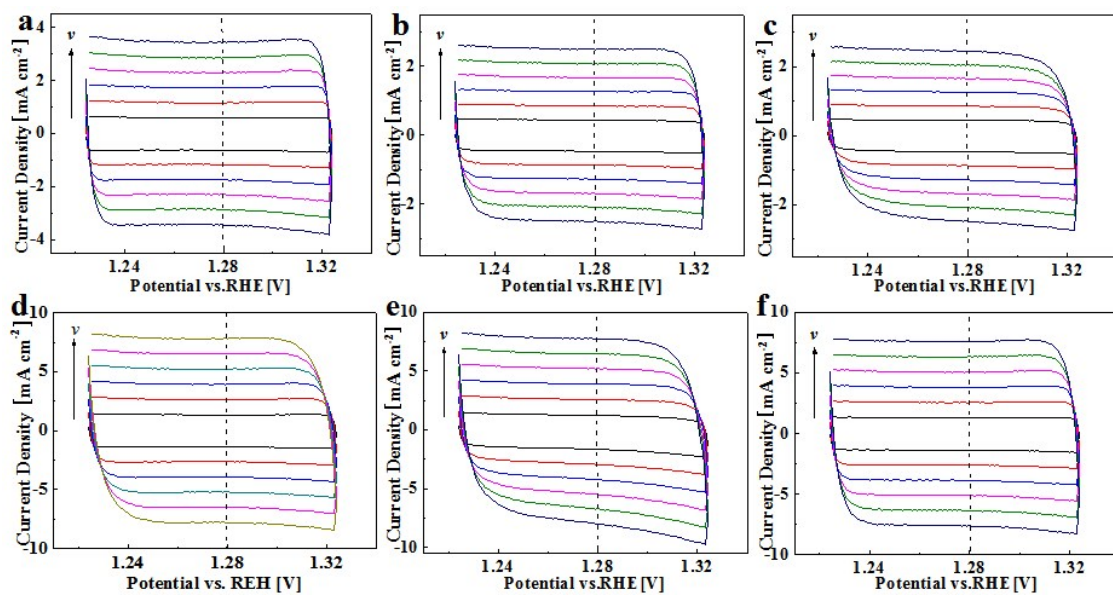


**Fig. S15.** CV curves obtained with different scan rates of 20, 40, 60, 80, 100 and 120  $\text{mV s}^{-1}$ : (a) Co-LDHs-1, (b) Co-LDHs-2, (c) cage-like Co-LDHs obtained by a cycling transformation route, (d) *d*-Co-LDHs-1, (e) *d*-Co-LDHs-2, and (f) disassembled cage-like Co-LDHs obtained by a cycling transformation route.

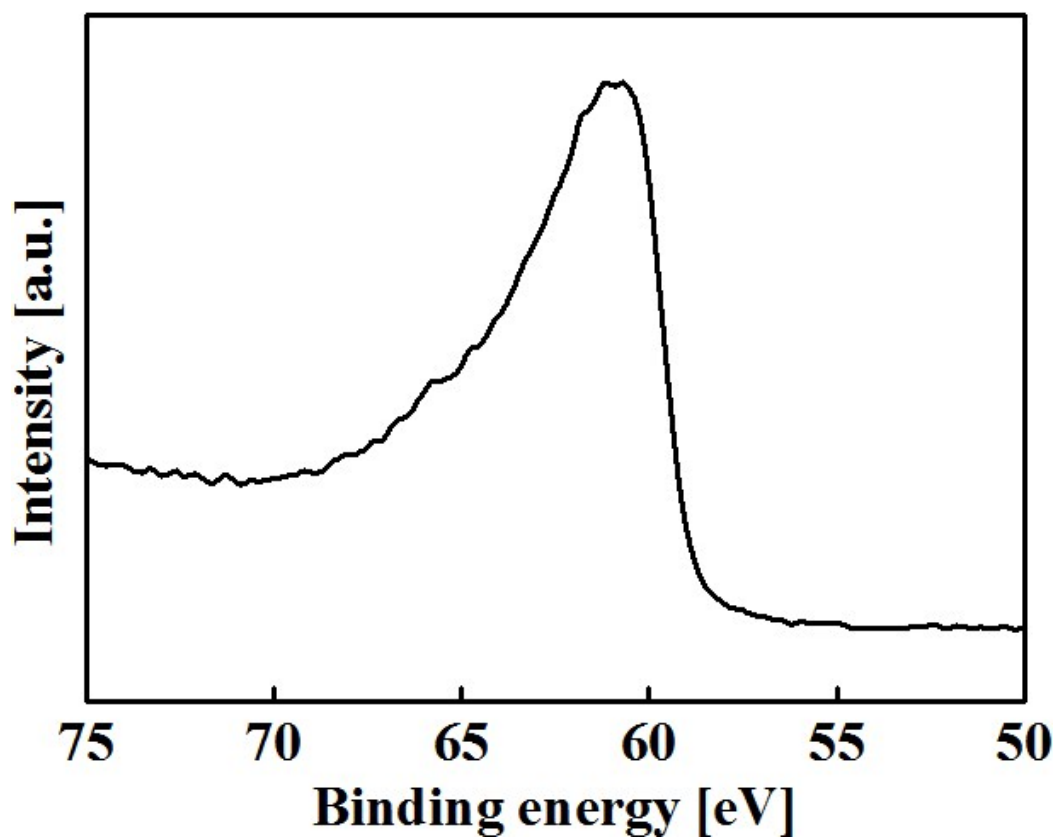


**Fig. S16.** High resolution XPS spectrum of Co-LDHs-1 collected in the region of from 50 to 75 eV. In the region, Fe3p binding energy peaked at  $\sim 53.7$  eV and  $\sim 55.6$  eV cannot be detected, signifying that Co-LDHs-1 are not be doped with Fe element.

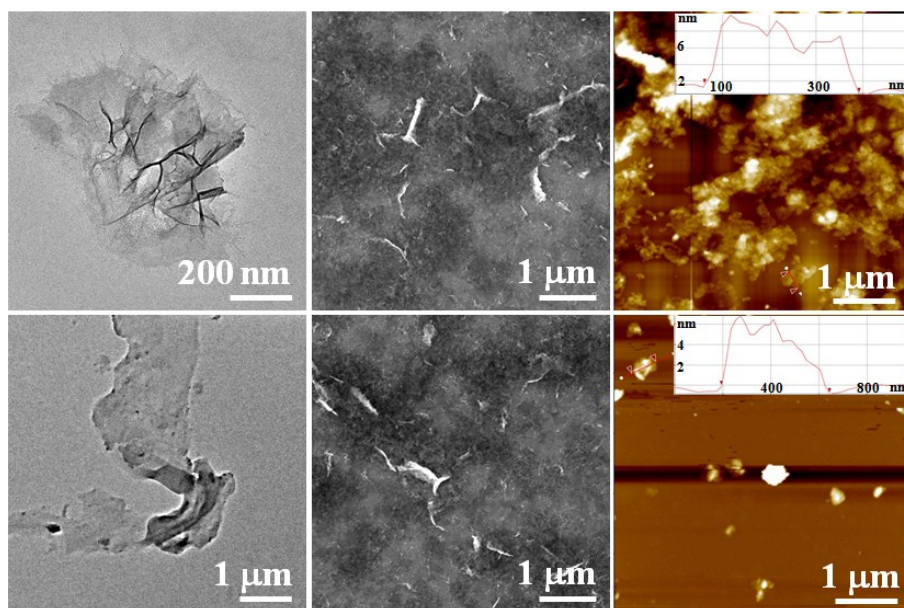


**Fig. S17.** *d*-Co-LDHs-1 (top), and *d*-Co-LDHs-2 (bottom). From left to right, TEM images, SEM images and AFM images of samples.

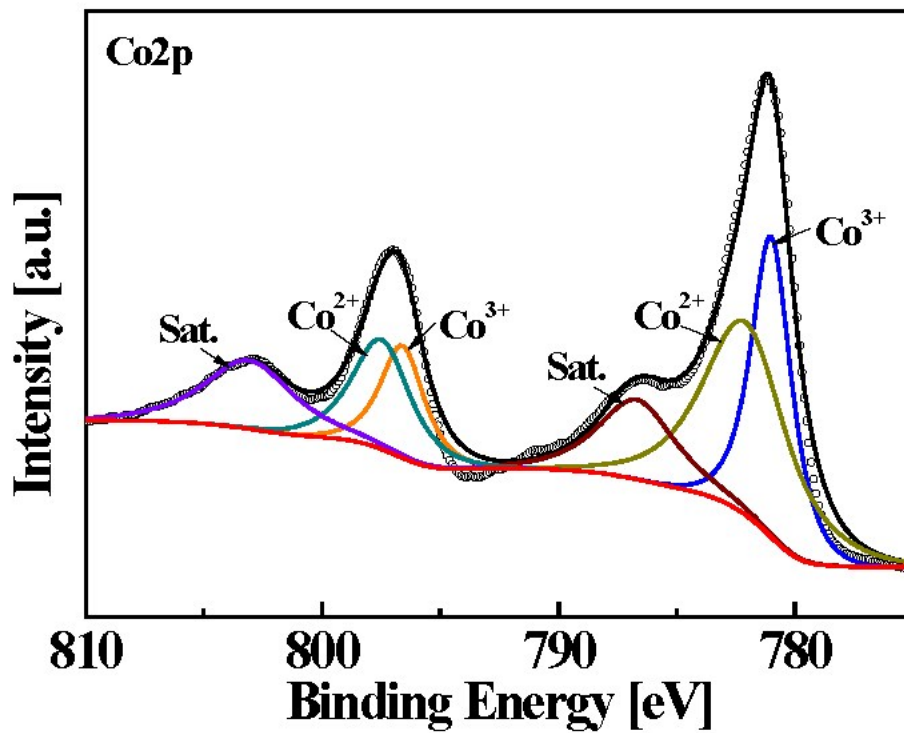
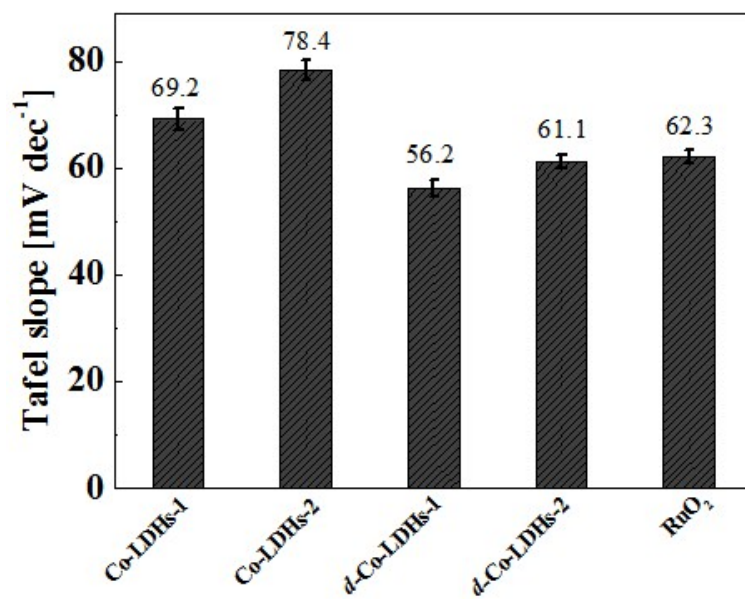
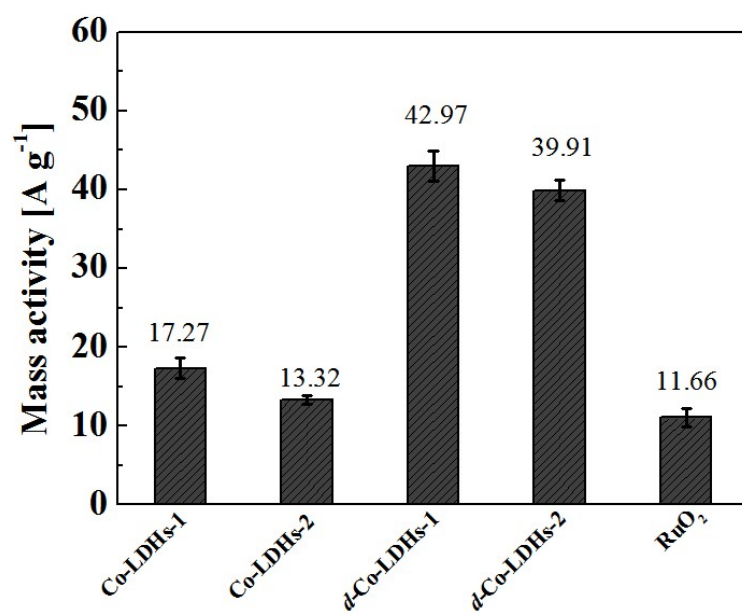


Fig. S18. XPS Co 2p spectra of *d*-Co-LDHs-1.



**Fig. S19.** The average Tafel plots of a series of Co-LDHs and RuO<sub>2</sub> originated from three independent *iR*-compensated LSV curves.



**Fig. S20.** Comparison of mass activity of a series of Co-LDHs and RuO<sub>2</sub> at an overpotential of 300 mV.

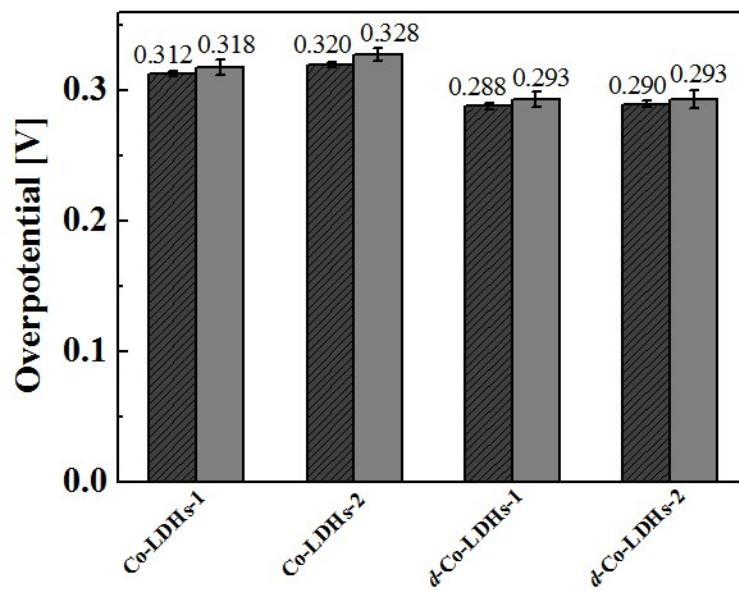


**Fig. S21.** Long-term stability tests of Co-LDHs loaded on GC electrodes via potential sweeps between 0.3 V and 0.6 V vs Hg/HgO with a scan rate of  $10 \text{ mV s}^{-1}$  for 3000 cycles.

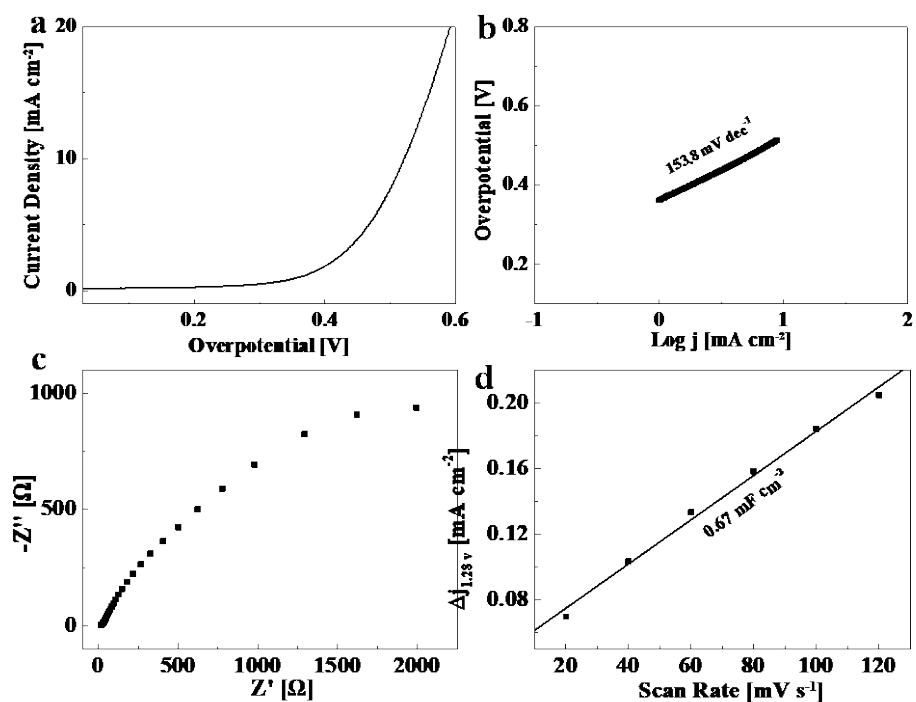


**Fig. S22.** Electrocatalytic performance of ZIF-67: (a) the  $iR$ -compensated LSV curves and (b) Tafel plots in 1 M KOH solution with a scan rate of  $5 \text{ mV s}^{-1}$ ; (c) Nyquist plots at overpotential of 395 mV and (d) the capacitive current densities as a function of scan rates of CV curves at potential of 1.28 V vs RHE.

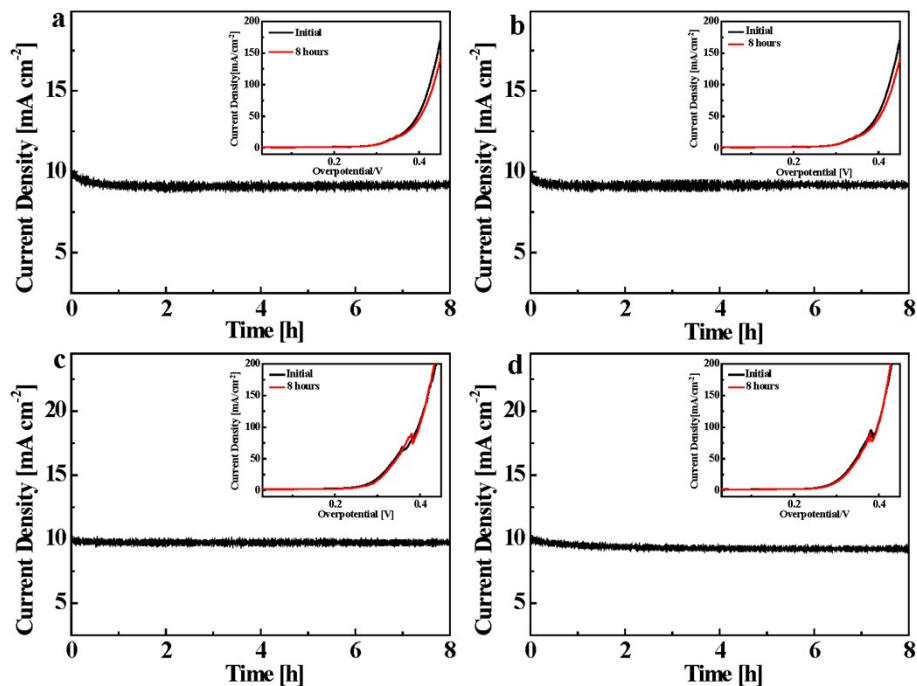


**Fig. S23.** Chronoamperometry tests of Co-LDHs loaded CFP electrodes to evaluate Co-LDH electrocatalyst stability: (a) Co-LDHs-1, (b) Co-LDHs-2, (c) *d*-Co-LDHs-1, and (d) *d*-Co-LDHs-2. Inset shows LSV curves before and after 8 hour's electrolysis.

The decrease of the current density of all electrodes is less than 10 % after 8 hours.

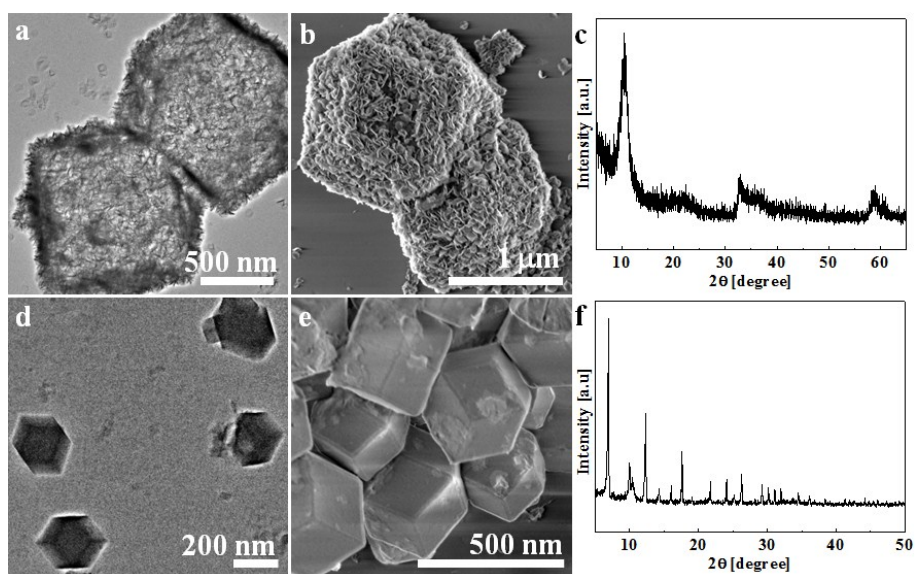


**Fig. S24.** TEM images and SEM images of (a, b) cage-like Co-LDHs and (d, e) ZIF-67 RDs prepared following a cycling transformation process (from non-purified Co-LDHs-1 to ZIF-67 to cage-like Co-LDHs; from non-purified ZIF-67 RDs to cage-like Co-LDHs to ZIF-67 RDs), respectively; corresponding XRD patterns of (c) cage-like of Co-LDHs and (f) ZIF-67 RDs.

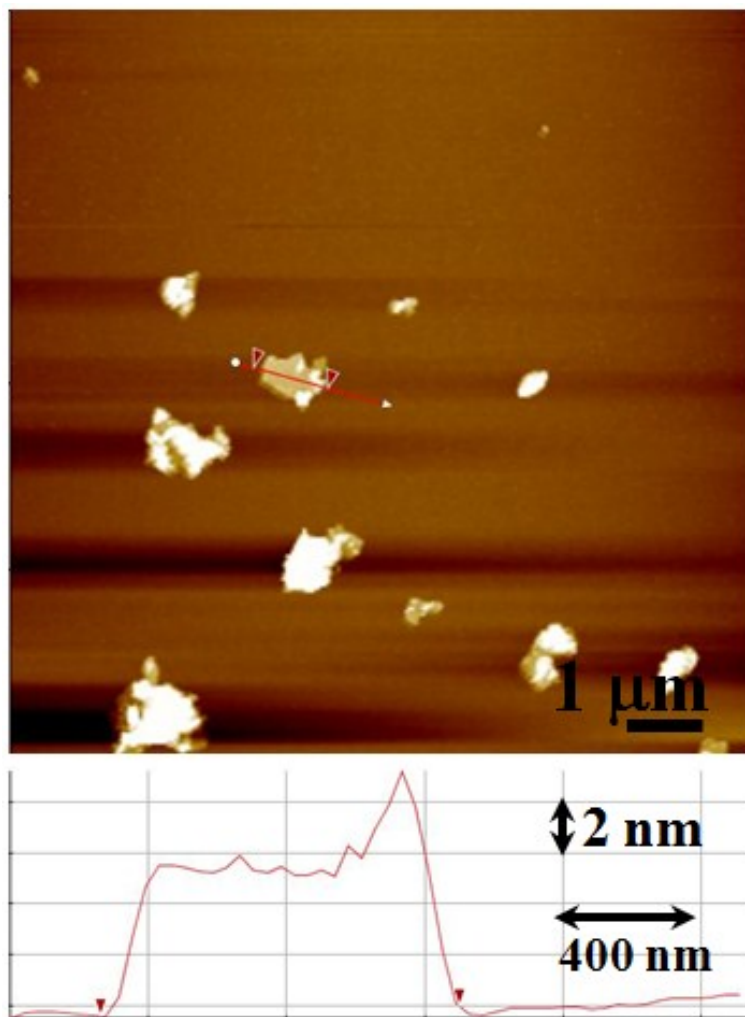


**Fig. S25.** AFM image of Co-LDH sheets that was prepared by suctioning the supernatant after sonication of the cage-like Co-LDHs prepared by a cycling transformation route in ethanol with a ultrasonic bath for 30 min and centrifugation at 3000 rpm.

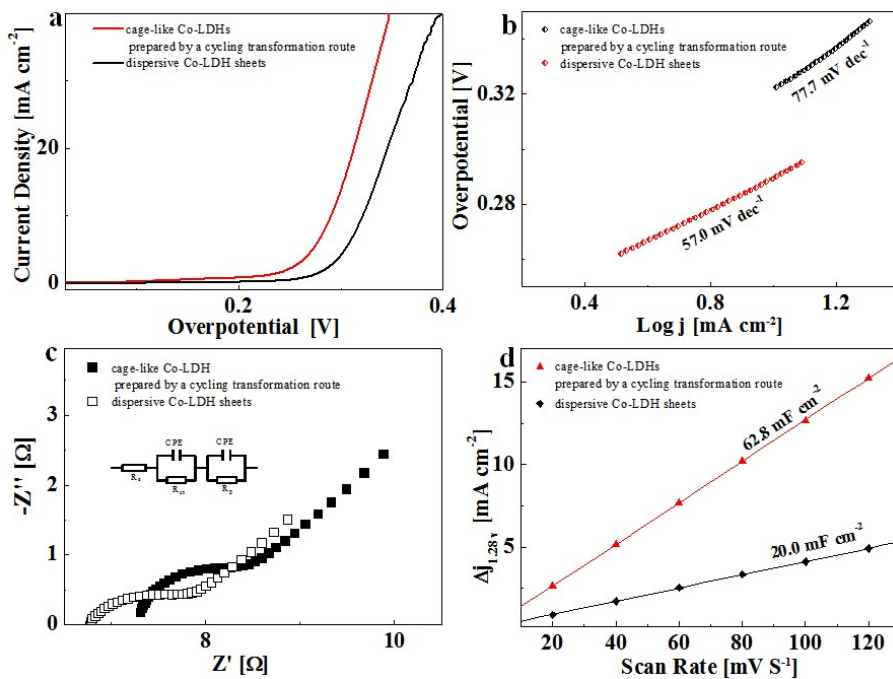


**Fig. S26.** Electrocatalytic performance of cage-like Co-LDHs prepared by a cycling transformation route and corresponding dispersive Co-LDH sheets. (a) The  $iR$ -compensated LSV curves and (b) Tafel plots in 1 M KOH solution with a scan rate of  $5 \text{ mV s}^{-1}$ ; (c) Nyquist plots at overpotential of 395 mV and (d) the capacitive current densities as a function of scan rates of CV curves at potential of 1.28 V.

Both electrodes of cage-like Co-LDHs and dispersive Co-LDH sheets give overpotentials of  $\eta_{10} = 321$  and  $290 \text{ mV}$ , Tafel slopes of  $77.7$  and  $57.0 \text{ mV dec}^{-1}$ ,  $R_{ct} = \sim 1.0$  and  $1.21 \text{ } \Omega$ , and capacitance values of  $20.0$  and  $62.8 \text{ mF cm}^{-2}$

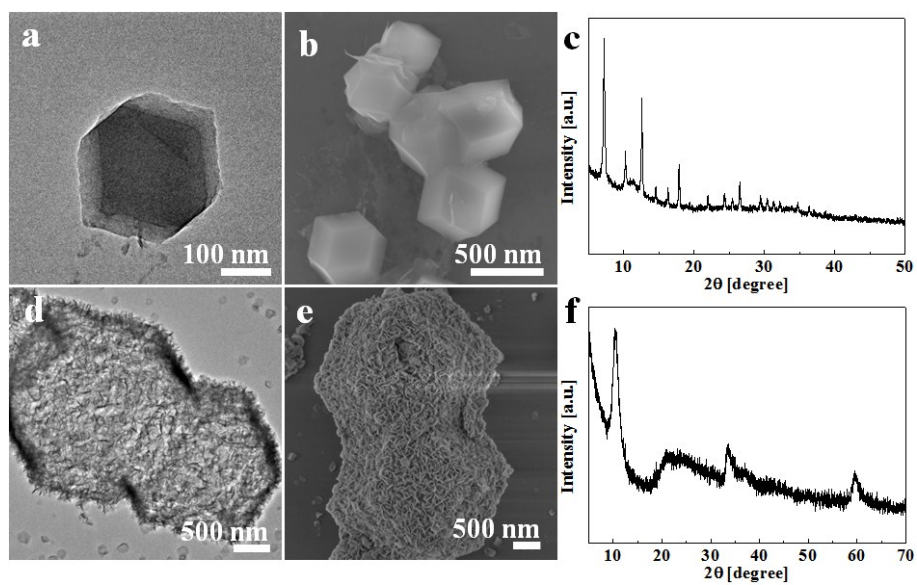


**Fig. S27.** TEM images and SEM images of (a, b) intermediate of ZIF-67 RDs and (d, e) final product of cage-like Co-LDHs prepared by cycling transformation of the used Co-LDHs, respectively; corresponding XRD patterns of (c) ZIF-67 RDs and (f) cage-like Co-LDHs.

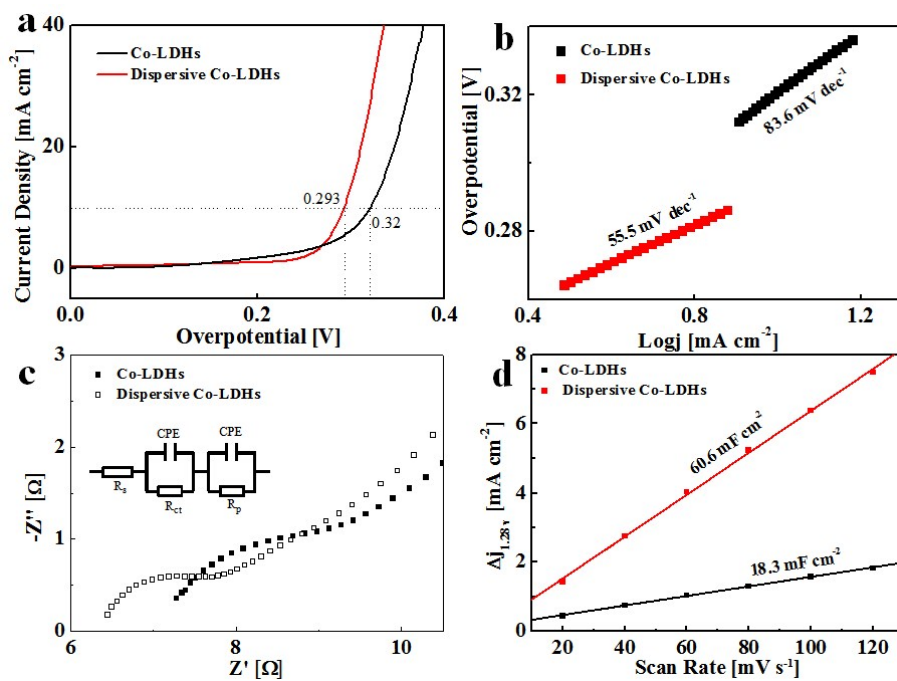


**Fig. S28.** Electrocatalytic performance of cage-like Co-LDHs prepared by cycling transformation of the used Co-LDHs and corresponding dispersive Co-LDH sheets. (a) The  $iR$ -compensated LSV curves and (b) Tafel plots in 1 M KOH solution with a scan rate of 5  $\text{mV s}^{-1}$ ; (c) Nyquist plots at overpotential of 395 mV and (d) the capacitive current densities as a function of scan rates of CV curves at potential of 1.28 V.

- 1 Y. Wang, Y. Zhang, Z. Liu, C. Xie, S. Feng, D. Liu, M. Shao and S. Wang, *Angew. Chem. Int. Ed.*, 2017, **56**, 5867-5871.
- 2 F. Song and X. Hu, *Nat. Commun.*, 2014, **5**, 4477.
- 3 W. Liu, J. Bao, M. Guan, Y. Zhao, J. Lian, J. Qiu, L. Xu, Y. Huang, J. Qian and H. Li, *Dalton Trans.*, 2017, DOI: 10.1039/C1037DT00906B.
- 4 J. Jiang, A. Zhang, L. Li and L. Ai, *J. Power Sources*, 2015, **278**, 445-451.
- 5 H. Liang, F. Meng, M. Caban-Acevedo, L. Li, A. Forticaux, L. Xiu, Z. Wang and S. Jin, *Nano Lett.*, 2015, **15**, 1421-1427.
- 6 Q. Yang, T. Li, Z. Lu, X. Sun and J. Liu, *Nanoscale*, 2014, **6**, 11789-11794.
- 7 F. Song and X. Hu, *J. Am. Chem. Soc.*, 2014, **136**, 16481-16484.
- 8 S. Chen, J. Duan, M. Jaroniec and S. Z. Qiao, *Angew. Chem. Int. Ed.*, 2013, **52**, 13567-13570.
- 9 C. Qiao, Y. Zhang, Y. Zhu, C. Cao, X. Bao and J. Xu, *J. Mater. Chem. A*, 2015, **3**, 6878-6883.
- 10 Y. Li, L. Zhang, X. Xiang, D. Yan and F. Li, *J. Mater. Chem. A*, 2014, **2**, 13250-13258.
- 11 D. Tang, Y. Han, W. Ji, S. Qiao, X. Zhou, R. Liu, X. Han, H. Huang, Y. Liu and Z. Kong, *Dalton Trans.*, 2014, **43**, 15119-15125.
- 12 P. F. Liu, S. Yang, B. Zhang and H. G. Yang, *ACS Appl. Mater. Interfaces*, 2016, **8**, 34474-34481.
- 13 W. Ma, R. Ma, C. Wang, J. Liang, X. Liu, K. Zhou and T. Sasaki, *ACS Nano*, 2015, **9**, 1977-1984.
- 14 J. Ping, Y. Wang, Q. Lu, B. Chen, J. Chen, Y. Huang, Q. Ma, C. Tan, J. Yang, X. Cao, Z. Wang, J. Wu, Y. Ying and H. Zhang, *Adv. Mater.*, 2016, **28**, 7640-+.
- 15 R. Liu, Y. Wang, D. Liu, Y. Zou and S. Wang, 2017, DOI: 10.1002/adma.201701546.